A comprehensive diagram to grow InAlN alloys by plasma-assisted molecular beam epitaxy

S. Fernández-Garrido,[a] Ž. Gačević, and E. Calleja
ISOM and Departamento de Ingeniería Electrónica, ETSI Telecomunicación Universidad Politécnica de Madrid, 28040 Madrid, Spain

(Received 22 September 2008; accepted 24 October 2008; published online 12 November 2008)

Indium incorporation and surface morphology of InAlN layers grown on (0001) GaN by plasma-assisted molecular beam epitaxy were investigated as a function of the impinging In flux and the substrate temperature in the 450–610 °C range. In incorporation was found to decrease with substrate temperature due to thermal decomposition of the growing layer, while for a given temperature it increased with the impinging In flux until stoichiometry was reached at the growth front. The InN losses during growth followed an Arrhenius behavior characterized by an activation energy of 2.0 eV. A growth diagram highly instrumental to identify optimum growth conditions was established. © *2008 American Institute of Physics*. [DOI: 10.1063/1.3026541]

InAlN alloys have a direct band gap tunable from 0.7 to 6.2 eV, and for a 17% In there is lattice match (in-plane) to GaN. Heterostructures and devices including InAlN layers, such as resonant cavities, multiquantum wells for high-speed intersubband devices, or high electron mobility transistors, have been recently reported.[1–4]

Growth diagrams, useful to identify optimum conditions, have been established for binaries (AlN, GaN, InN), grown by plasma-assisted molecular beam epitaxy (PA-MBE), from the surface morphology dependence on growth temperature and impinging fluxes.[5–8] However, the growth of InAl(Ga)N alloys poses much more difficulties due to InN thermal decomposition[9–12] and strong differences between InN and AlN.

This work reports on the growth and characterization of metal-face InAlN layers on GaN templates. Indium incorporation and surface morphology are analyzed as a function of growth temperature and metal fluxes to build up a growth diagram.

InAlN thin layers (~80 nm thick) were grown by PA-MBE on (0001) GaN templates (~3.6 μm thick) grown by metal-organic vapor phase epitaxy on sapphire (Lumilog). Growth temperature was measured with an Ircon Modline3 optical pyrometer. Metal fluxes (Φ_{Ga}, Φ_{Al}, Φ_{In}), measured as beam equivalent pressure (Bayard Alpert), were calibrated in atoms/s cm^2 using cross-sectional scanning electron microscopy (SEM) data from N-rich GaN, AlN, and InN thick layers grown at temperatures where thermal decomposition and adatom desorption are negligible.[5] Similarly, the active N flux Φ_N was calibrated in atoms/s cm^2 using cross-sectional SEM data from Ga-rich GaN thick layers grown at low temperatures (680 °C). Prior to the InAlN growth, a 100 nm thick GaN buffer layer was grown at 700 °C under intermediate Ga-rich conditions[5] to obtain a smooth and flat surface. Alloy compositions were assessed by high resolution x-ray diffraction (HR-XRD) and surface morphologies were characterized by SEM (JEOL JSM-5800) and by atomic force microscopy (AFM) (Digital Instruments MMAFM-2).

To analyze separately the effects of growth temperature and impinging In flux on In incorporation, two sets of samples were grown. In a first set (series A) all impinging fluxes were kept constant and the growth temperature varied between 450 and 610 °C, a range where Al sticking coefficient is 1, being preferentially incorporated due to a much higher energy of the Al–N bond than that of In–N.[9,11] The III/V flux ratio was <1(N-rich) with impinging fluxes of $\Phi_{Al}=2.7\pm0.1\times10^{14}$ atoms/s cm^2, $\Phi_{In}=1.2\pm0.1\times10^{14}$ atoms/s cm^2, and $\Phi_N=4.2\pm0.1\times10^{14}$ atoms/s cm^2. A 0.31 ± 0.03 nominal InN mole fraction is derived from $\Phi_{In}/(\Phi_{In}+\Phi_{Al})$.[9] In series B the growth temperature was set at 535 °C and Φ_{In} was varied while keeping the same Φ_{Al} and Φ_N of series A.

Figure 1(a) shows a continuous decrease in the *actual* InN mole fraction $[InN]^*$ (series A) with the growth temperature, from the nominal value (considering the experimental error derived from the calibration of the impinging fluxes) 0.33 at 450 °C down to 0.02 at 607 °C. For temperatures below 500 °C In droplets were not observed upon growth termination because the growth was carried out under N excess. However, for temperatures in the 500–585 °C range In droplets were observed. The reason is that, for temperatures above ~500 °C, InN decomposition provides excess In that partially reincorporates into the crystal until effective stoichi-

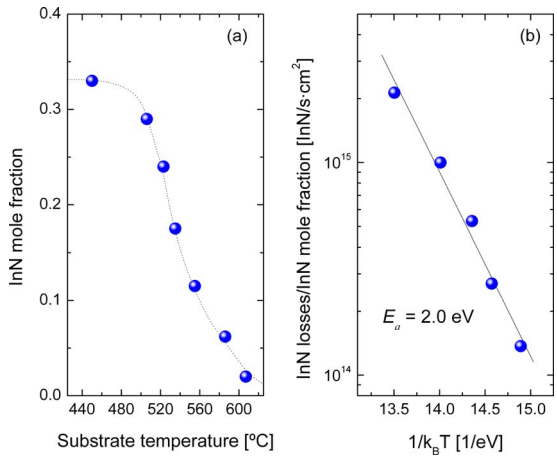

FIG. 1. (Color online) (a) InN mole fraction $[InN]^*$ as a function of the substrate temperature for $\Phi_{Al}=2.7\times10^{14}$ atoms/s cm^2, $\Phi_{In}=1.2\times10^{14}$ atoms/s cm^2, and $\Phi_N=4.2\times10^{14}$ atoms/s cm^2. (b) Arrhenius plot of the InN losses normalized to $[InN]^*$ values for those samples grown in the 500–585 °C temperature range (In-droplets region). The activation energy for InN losses is 2.0 ± 0.2 eV.

[a]Electronic mail: sfernandez@die.upm.es.

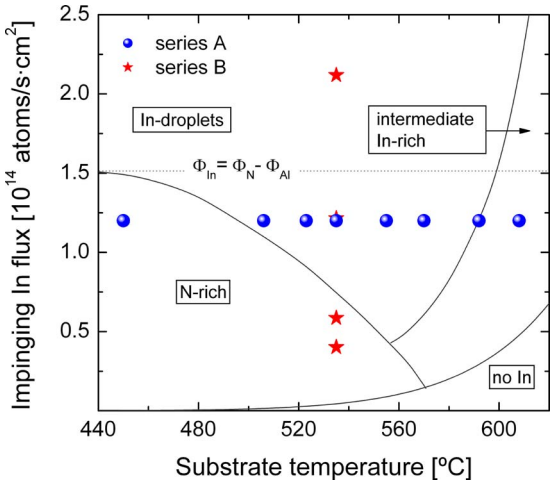

FIG. 2. (Color online) The PA-MBE growth diagram for metal-face InAlN. Four different growth regimes are distinguished: In-droplets, intermediate In-rich, N-rich, and no In. The closed symbols define the conditions used for the InAlN layers grown in this study. The horizontal dotted line, labeled as $\Phi_{In}=\Phi_N-\Phi_{Al}$, represents the Φ_{In} value required to reach stoichiometry in terms of impinging fluxes.

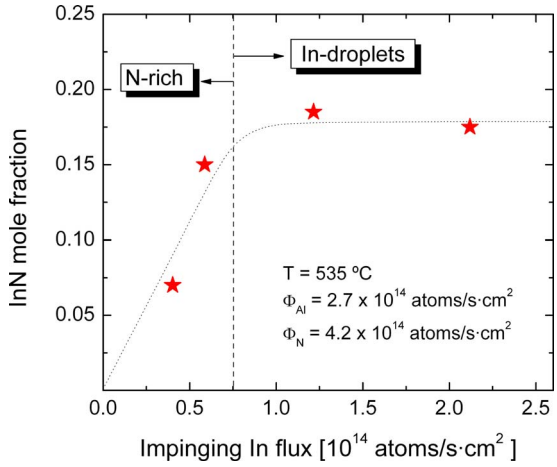

FIG. 3. (Color online) InN mole fraction $[InN]^*$ as a function on the impinging In flux at 535 °C for $\Phi_{Al}=2.7\times10^{14}$ atoms/s cm^2 and $\Phi_N=4.2\times10^{14}$ atoms/s cm^2.

ometry (at the growth front) is reached (growth starts under N-rich conditions). Beyond this point the excess In generates droplets at the surface that eventually disappear by desorption at high enough temperatures (>585 °C).[7,13] The growth is then limited by N, and the $[InN]^*$ value is lower than the nominal one by an amount that increases with the growth temperature [Fig. 1(a)]. These morphology changes are similar to those reported by Gallinat *et al.*[7] for In-face InN.

As in InGaN alloys,[9] we may expect that, under steady state conditions, InN losses (Φ_{InN}^{losses}) by thermal decomposition are proportional to the Boltzmann factor with an activation energy E_a and to $[InN]^*$ with a constant factor C,

$$\Phi_{InN}^{losses}(T) = C \times [InN]^* \times \exp(-E_a/k_BT). \quad (1)$$

The nominal In incorporation rate Φ_{In}^{inc} within the 500–585 °C temperature range, (In-droplets region) when decomposition and desorption are not considered (ideal case), equals $(\Phi_N-\Phi_{Al})$.[9] When decomposition and desorption are considered, an actual In incorporation rate can be defined $\Phi_{In}^{inc^*}$, which relates to the $[InN]^*$ value. The Φ_{InN}^{losses} were estimated within this temperature range as the $\Phi_{In}^{inc}-\Phi_{In}^{inc^*}$ difference being the latter derived from HR-XRD data: $[InN]^*=\Phi_{In}^{inc^*}/(\Phi_{In}^{inc^*}+\Phi_{Al})$. Figure 1(b) shows an Arrhenius plot of Φ_{InN}^{losses} normalized to $[InN]^*$ values, which yield C and E_a values [best fit to Eq. (1)] of 1.27×10^{27} InN/s cm^2 and 2.0 eV, respectively. This energy value is in good agreement with both the In–N bond energy, 1.93 eV,[14] and the activation energy for thermal decomposition of In-face InN, 1.92 eV.[7]

Figure 2 shows a growth diagram for metal-face InAlN determined from the temperature dependences of both Φ_{InN}^{losses} [Eq. (1)] and In desorption rates from liquid In.[7] Notice that the diagram is also qualitatively valid for different values of the impinging metal and N fluxes. The horizontal dotted line, labeled as $\Phi_{In}=\Phi_N-\Phi_{Al}$, represents the nominal Φ_{In} value required to reach stoichiometric conditions for the given values of Φ_N and Φ_{Al}, when neither In desorption nor InN decomposition are considered. The selected value of Φ_{In} for series A is lower, indicating nominal N-rich conditions. Four different regimes are distinguished as a function of the impinging flux Φ_{In} and the substrate temperature, namely, N-rich, In-droplets, intermediate In-rich, and no In, that is, where In incorporation is negligible. The solid line starting at low temperatures, that separates N-rich and In-droplets regimes, departs from the horizontal dotted line because excess In is available at the growth front due to InN decomposition. As temperature increases, more In excess is available; thus, less impinging Φ_{In} is required for stoichiometry conditions. Above this solid line, the In excess cannot be neither desorbed (below ~560 °C) nor incorporated to the crystal because of N shortage; thus, it accumulates on the surface as droplets. The stoichiometry condition determined by this solid line is given by

$$\Phi_{In} + \Phi_{InN}^{losses}(T) = \Phi_N - \Phi_{Al}. \quad (2)$$

For temperatures above 560 °C, In desorption becomes non-negligible, opening a window in which growth can proceed under intermediate In-rich conditions.[9,11,12] As in the case of In(Al)GaN alloys the best quality is expected for those samples grown in this regime due to the presence of a surfactant In adlayer with coverages ranging from 0 (lower N-rich boundary) to 2.5 ML (upper In-droplet boundary).[7,9,11–13] Within this window (between the two solid lines) the required Φ_{In} increases with temperature to compensate In desorption. The lower boundary (toward N-rich) represents strict stoichiometry, whereas the upper one (toward In-droplets) is slightly metal rich. Both solid lines follow the expression

$$\Phi_{In} + \Phi_{InN}^{losses}(T) - \Phi_{In}^{des}(T) = \Phi_N - \Phi_{Al}, \quad (3)$$

where $\Phi_{In}^{des}(T)$ reaches its maximum value (for a given temperature) at the upper boundary. These maximum values follow an Arrhenius temperature dependence with an activation energy of 2.49 eV.[7] The region where In incorporation is negligible arises from InN losses higher than the In incorporation rate limited by the impinging fluxes.

The diagram in Fig. 2 clearly shows that, for a given set of metals and N fluxes, the alloy composition changes significantly with the growth temperature. In addition, for a given temperature, the alloy composition is also expected to change with Φ_{In} outside the In-droplets regime. Figure 3 shows the increase in $[InN]^*$ as a function of Φ_{In} for series B.

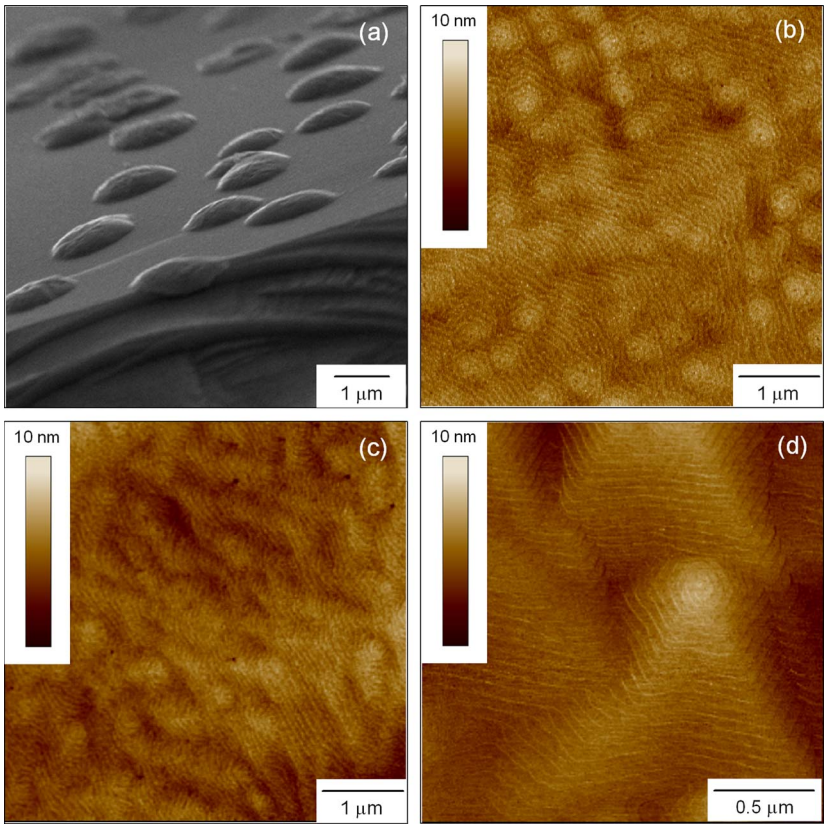

FIG. 4. (Color online) Representative surface morphologies of InAlN samples grown within the different growth regimes with $\Phi_{Al}=2.7\times10^{14}$ atoms/s cm^2 and $\Phi_N=4.2\times10^{14}$ atoms/s cm^2: (a) In-droplets ($T=535$ °C, $\Phi_{In}=2.1\times10^{14}$ atoms/s cm^2), (b) intermediate In-rich ($T=592$ °C, $\Phi_{In}=1.2\times10^{14}$ atoms/s cm^2), and (c) N rich ($T=535$ °C, $\Phi_{In}=0.6\times10^{14}$ atoms/s cm^2). (d) AFM image of a GaN sample grown under Ga-rich conditions near the thermodynamical limit for Ga-droplets formation.

When stoichiometry is reached at the growth front (solid line boundary in Fig. 2), $[InN]^*$ reaches its maximum value, beyond which In droplets develop while $[InN]^*$ remains constant.

Figure 4 shows the characteristic surface morphologies for samples grown at different regimes. Figure 4(a) shows 1–2 μm size In droplets due to In accumulation (In-droplets regime). Figures 4(b) and 4(c) show 5×5 μm^2 AFM images of samples grown in the intermediate In-rich and N-rich regimes, respectively. In the intermediate In-rich regime smooth surfaces with average roughness (rms) of 0.5 to 0.8 nm were observed. As shown in Fig. 4(b) the surface is characterized by atomic steps and spiral hillocks like those typical of the dislocation pinned step-flow growth of GaN layers grown by PA-MBE under Ga-rich conditions [see Fig. 4(d)]. Surprisingly, as shown in Fig. 4(c), for those samples grown in the N-rich regime smooth surfaces with atomic steps and rms values below 0.8 nm were obtained instead of the rough surfaces normally observed for III-N layers grown under N-rich conditions[5–8]

In summary, In incorporation into InAlN layers grown by PA-MBE was analyzed as a function of the growth temperature and the impinging In flux. The In incorporation into the layers was found to decrease with the substrate temperature due to thermal InN decomposition and to increase with the impinging In flux until stoichiometry was reached at the growth front. From the temperature dependences of both InN losses and In desorption rates from liquid In, a growth diagram was constructed showing four different growth regimes: N-rich, In-droplets, intermediate In-rich, and a fourth one where In incorporation is negligible. This diagram provides a useful guide to control both alloy composition and surface morphology of InAlN layers grown by PA-MBE.

We acknowledge fruitful discussions with J. Pereiro, A. Bengoechea, J. Grandal, M. Utrera, and A. Redondo-Cubero. This work was partially supported by research grants from the Spanish Ministry of Education (Grant No. NAN04/09109/C04/2, Consolider-CSD 2006-19) and the Community of Madrid (Grant No. S-0505/ESP-0200).

[1] J. Dorsaz, J.-F. Carlin, S. Gradecak, and M. Ilegems, J. Appl. Phys. **97**, 084505 (2005).
[2] G. Cywinski, C. Skierbiszewski, A. Feduniewicz-Zmuda, M. Siekacz, L. Nevou, L. Doyennette, M. Tchernycheva, F. H. Julien, P. Prystawko, M. Krysko, S. Grzanka, I. Grzegory, A. Presz, J. Z. Domagala, J. Smalc, M. Albrecht, T. Remmele, and S. Porowski, J. Vac. Sci. Technol. B **24**, 1505 (2006).
[3] M. Higashiwaki, T. Mimura, and T. Matsui, Jpn. J. Appl. Phys., Part 2 **45**, L843 (2006).
[4] Ž. Gačević, S. Fernández-Garrido, and E. Calleja (unpublished).
[5] B. Heying, R. Averbeck, L. F. Chen, E. Haus, H. Riechert, and J. S. Speck, J. Appl. Phys. **88**, 1855 (2000).
[6] G. Koblmueller, R. Averbeck, L. Geelhaar, H. Riechert, W. Hösler, and P. Pongratz, J. Appl. Phys. **93**, 9591 (2003).
[7] C. S. Gallinat, G. Koblmüller, J. S. Brown, and J. S. Speck, J. Appl. Phys. **102**, 064907 (2007).
[8] G. Koblmüller, S. Fernández-Garrido, E. Calleja, and J. S. Speck, Appl. Phys. Lett. **91**, 161904 (2007).
[9] R. Averbeck and H. Riechert, Phys. Status Solidi A **176**, 301 (1999).
[10] S. Schmult, T. Siegrist, A. M. Sergent, M. J. Manfra, and R. J. Molnar, Appl. Phys. Lett. **90**, 021922 (2007).
[11] E. Monroy, N. Cogneau, D. Jalabert, E. Bellet-Amalric, Y. Hori, F. Enjalbert L. S. Dang, and B. Daudin, Appl. Phys. Lett. **82**, 2242 (2003).
[12] S. Fernández-Garrido, A. Redondo-Cubero, R. Gago, F. Bertram, J. Christen, E. Luna, A. Trampert, J. Pereiro, E. Muñoz, and E. Calleja, J. Appl. Phys. **104**, 083510 (2008).
[13] E. Monroy, B. Daudin, E. Bellet-Amalric, N. Cogneau, D. Jalabert, F. Enjalbert, J. Brault, J. Barjon, and L. S. Dang, J. Appl. Phys. **93**, 1550 (2003).
[14] J. H. Edgar, *Group-III Nitrides* (INSPEC, London, 1994).